Kinetic lattice Boltzmann method for microscale gas flows: Issues on boundary condition, relaxation time, and regularization

Xiao-Dong Niu,* Shi-Aki Hyodo, and Toshihisa Munekata
Computational Physics Laboratory Toyota Central R&D Laboratories, Inc., Nagakute, Aichi, 480-1192, Japan

Kazuhiko Suga
Department of Mechanical Engineering, Osaka Prefecture University, Sakai 599-8531, Japan
(Received 7 May 2007; published 27 September 2007)

It is well known that the Navier-Stokes equations cannot adequately describe gas flows in the transition and free-molecular regimes. In these regimes, the Boltzmann equation (BE) of kinetic theory is invoked to govern the flows. However, this equation cannot be solved easily, either by analytical techniques or by numerical methods. Hence, in order to efficiently maneuver around this equation for modeling microscale gas flows, a kinetic lattice Boltzmann method (LBM) has been introduced in recent years. This method is regarded as a numerical approach for solving the BE in discrete velocity space with Gauss-Hermite quadrature. In this paper, a systematic description of the kinetic LBM, including the lattice Boltzmann equation, the diffuse-scattering boundary condition for gas-surface interactions, and definition of the relaxation time, is provided. To capture the nonlinear effects due to the high-order moments and wall boundaries, an effective relaxation time and a modified regularization procedure of the nonequilibrium part of the distribution function are further presented based on previous work [Guo *et al.*, J. Appl. Phys. **99**, 074903 (2006); Shan *et al.*, J. Fluid Mech. **550**, 413 (2006)]. The capability of the kinetic LBM of simulating microscale gas flows is illustrated based on the numerical investigations of micro Couette and force-driven Poiseuille flows.

DOI: 10.1103/PhysRevE.76.036711 PACS number(s): 47.11.−j, 51.10.+y

I. INTRODUCTION

Gas flows in microscale devices have received particular attention over the past decade with the rapid development in microelectromechanical systems (MEMS) [1–3]. In these microscale devices, the flows are usually distinguished by relatively small Mach numbers ($\mathrm{Ma}=U/c_s \leq 0.3$, where U is the characteristic velocity of the flow and c_s is the sound speed) and large Knudsen numbers ($\mathrm{Kn}=\lambda/H \geq 0.01$, where λ is the molecular mean free path of fluid and H is the characteristic length of the flow domain). It is well known that processes in these kinds of flows are described by the Boltzmann equation (BE) of the kinetic theory [4,5]. Since the numerical solution of the BE, either directly [6] or via the direct simulation Monte Carlo (DSMC) method [7], is very time expensive, there is a strong desire for accurate models which allow simulations of processes in microscale gas flows at lower computational cost.

Currently, there are three well-known approaches toward this goal, the Chapman-Enskog (CE) method [4,5,8], the Grad's moment method [9–11], and the lattice Boltzmann method (LBM) [12,13]. In the CE method, the phase density is expanded in powers of Kn, and to different successive orders the expansion yields the Euler, Navier-Stokes (NS), Burnett equations, and so on. The NS equations cease to be accurate for Kn larger than 0.01, and although the Burnett equations are theoretically valid for larger Knudsen numbers, their numerical solutions become linearly unstable for processes involving small wavelength or high frequencies [14].

In the Grad's moment method [9–11], the BE is replaced by a set of moment equations, first-order partial differential equations for the moments of the distribution function. For the closure of the equations, the phase density is approximated by a expansion in the Hermite orthogonal polynomials about local Maxwellian equilibrium distribution, and the coefficients of the polynomials are related to the moments. Only a few moments have an intuitive physical meaning, i.e. density, momentum density, energy density, heat flux, and pressure tensor. The set of 13-moments forms the basis of Grad's well-known 13-moment equations [9]. However, the 13-moment set does not allow the computation of Knudsen boundary layers [15,16] and, with an increasing number of moments [17], the Knudsen boundary layers can be computed, but solving these moment equations becomes formidable due to its complexities.

The LBM [12,13] is a simplified solver of the BE on a discrete lattice. The LBM is originated from the lattice gas cellular automaton models [18–20], and quickly accepted as an efficient computational fluid dynamics (CFD) solver [21] due to its distinctive computational features: easy to implement, intrinsically parallelizable, and straightforward for handling complex geometries. Because of its intrinsic kinetic nature, the LBM seems to allow the microscopic physics responsible for many complex fluid phenomena to be modeled more directly [22–28]. However, since the early LBM models only satisfy the rotational invariance of hydrodynamic properties up to the Navier-Stokes order, an argument [29] usually arises, especially when they are applied in simulations of high-Knudsen number flows [30–39], in which the higher-order moments are manifested.

Recently, inspired by the Grad's moment method, a rigorous and systematic theoretical procedure for the LBM, in-

*Author to whom correspondence should be addressed; e1351@mosk.tytlabs.co.jp

cluding effects of the higher-order moments, was developed [40]. By using the Hermite expansion approach, hydrodynamic moments at various orders can be precisely and explicitly determined at a given order of truncations of the Hermite polynomials. On this point, one can think that the LBM is equivalent to the Grad moment method.

In this paper, we further develop the above kinetic theory of the LBM by addressing the issues of the boundary condition, the relaxation time, and the nonequilibrium moments. In Sec. II, we give a brief description of the lattice Boltzmann equation (LBE) including higher-order moment effects [40]. The accuracy issue required by describing fluid properties is discussed. In Sec. III, three main topics are further discussed; first, the boundary condition. Derivation of the diffuse scattering boundary condition [30,41,42] on the Hermite basis is presented. Second, we discuss the relaxation time. In the presence of the solid wall, an effective relaxation time is introduced. The last topic is related to the nonequilibrium distribution. To preserve the nonequilibrium hydrodynamic moments, a regularization procedure [38,43] of the nonequilibrium distribution is discussed, and its effects on the Knudsen layer are highlighted. Sec. IV is devoted to the numerical illustrations of the LBM in simulating the high-Knudsen number flows and concluding remarks are given in Sec. V.

II. LBE WITH HIGHER-ORDER MOMENTS

The BE [4,5] has been well accepted as a mathematical model simulating the microscale fluidic gas in the entire Knudsen regime. The BE describes evolutions of a single particle velocity distribution function $f(\mathbf{x},\boldsymbol{\xi},t)$ in the phase space $(\mathbf{x},\boldsymbol{\xi})$, where $\mathbf{x}$ denotes the position and $\boldsymbol{\xi}$ denotes the velocity of the particle, and can be written as the following BGK form:

$$\frac{\partial f}{\partial t} + \boldsymbol{\xi}\cdot\nabla f + \mathbf{a}\cdot\nabla_{\boldsymbol{\xi}} f = -\frac{f - f^{(0)}}{\tau}. \tag{1}$$

Here, τ is the characteristic relaxation time of collisions to equilibrium, $\nabla_{\boldsymbol{\xi}}$ the gradient operator in velocity space, and $\mathbf{a}$ the acceleration due to the external or self-generated body force. $f^{(0)}$ represents a local equilibrium distribution and is the Maxwellian

$$f^{(0)} = \frac{\rho}{(2\pi RT)^{D/2}}\exp\left(-\frac{(\boldsymbol{\xi}-\mathbf{u})^2}{2RT}\right), \tag{2}$$

where ρ, T, and $\mathbf{u}$ are the fluid density, temperature, and velocity, respectively, D is the dimension of the space, and R is the gas constant. Hydrodynamic variables, such as the density, velocity, and temperature are defined, respectively, as in the following form:

$$\rho = \int f d\boldsymbol{\xi}, \quad \rho\mathbf{u} = \int f\boldsymbol{\xi} d\boldsymbol{\xi}, \quad D\rho RT + \rho\mathbf{u}^2 = \int f\boldsymbol{\xi}^2 d\boldsymbol{\xi}. \tag{3}$$

As argued by Grad [9], the Boltzmann BGK equation (1) can be projected onto the Hermite orthogonal basis and we have [40]

$$\frac{\partial f_\alpha}{\partial t} + \boldsymbol{\xi}_\alpha\cdot\nabla f_\alpha = -\frac{f_\alpha - f_\alpha^{(0)}}{\tau} + F_\alpha, \tag{4}$$

where $F_\alpha = -\mathbf{a}\cdot\nabla_{\boldsymbol{\xi}_\alpha} f_\alpha$ is the contribution of the force term, and $f_\alpha^{(0)}$ is the nth-order truncated Hermite expansion of the Maxwellian distribution (2) at a set of discrete velocities $\boldsymbol{\xi}_\alpha$ ($\alpha = 0,1,2,\ldots,d$, and d depending the truncation order N of the Hermite expansion) and is written as

$$f_\alpha^{(0)} = \omega_\alpha \sum_{n=0}^{N} \frac{1}{n!} a_0^{(n)} H^{(n)}(\boldsymbol{\xi}_\alpha), \tag{5}$$

where $a_0^{(n)} \approx \Sigma_{\alpha=1}^{d} f_\alpha^{(0)} H^{(n)}(\boldsymbol{\xi}_\alpha)$ is the Hermite expansion coefficient, ω_α is the weight function, and $H^{(n)}(\boldsymbol{\xi}_\alpha)$ is the nth-order Hermite polynomial, the first few terms of which can be expressed as

$$H^{(0)}(\boldsymbol{\xi}_\alpha) = 1,$$

$$H^{(1)}(\boldsymbol{\xi}_\alpha) = \boldsymbol{\xi}_{\alpha i},$$

$$H^{(2)}(\boldsymbol{\xi}_\alpha) = \boldsymbol{\xi}_{\alpha_i}\boldsymbol{\xi}_{\alpha_j} - \delta_{i,j},$$

$$H^{(3)}(\boldsymbol{\xi}_\alpha) = \boldsymbol{\xi}_{\alpha_i}\boldsymbol{\xi}_{\alpha_j}\boldsymbol{\xi}_{\alpha_k} - \boldsymbol{\xi}_{\alpha_i}\delta_{jk} - \boldsymbol{\xi}_{\alpha_j}\delta_{ik} - \boldsymbol{\xi}_{\alpha_k}\delta_{i,j}, \tag{6}$$

where δ_{ij} is the Kronecker delta function. In the discrete velocity space, the fluid variables are calculated as

$$\rho = \sum_{\alpha=0}^{d} f_\alpha, \quad \rho\mathbf{u} = \sum_{\alpha=0}^{d} f_\alpha\boldsymbol{\xi}_\alpha, \quad D\rho RT + \rho\mathbf{u}^2 = \sum_{\alpha=0}^{d} f_\alpha\boldsymbol{\xi}_\alpha^2. \tag{7}$$

Obviously from Eqs. (4)–(7), the truncation level of the Hermite expansion determines the accuracy of Eq. (4) to approximate Eq. (1), and the level of accuracy is increased as higher-order terms in the truncated expansion are retained. As revealed by the CE method, by retaining up to the fourth-order terms in the Hermite expansion, the Burnett level accuracy pertaining to the fluid momentum evolution for isothermal systems can be satisfied. For most microscale gas flows in MEMS [1–3], the Burnett description is said to be accurate enough for modeling them. For isothermal MEMS fluids, a third-order Hermite expansion is enough to model the momentum equation at the Burnett level due to the small Mach numbers and the equilibrium distribution function $f_\alpha^{(0)}$ has the following form [40]:

$$f_\alpha^{(0)}(\mathbf{x},t) = \omega_\alpha\rho\left\{1 + \frac{\boldsymbol{\xi}_\alpha\cdot\mathbf{u}}{RT} + \frac{1}{2}\left[\frac{(\boldsymbol{\xi}_\alpha\cdot\mathbf{u})^2}{(RT)^2} - \frac{\mathbf{u}^2}{RT}\right] + \frac{1}{6}\left[\frac{(\boldsymbol{\xi}_\alpha\cdot\mathbf{u})^2}{(RT)^2} - 3\frac{\mathbf{u}^2}{RT}\right]\frac{\boldsymbol{\xi}_\alpha\cdot\mathbf{u}}{RT}\right\}. \tag{8}$$

Similarly, the force distribution term F_α in Eq. (4) can be written as

TABLE I. $D2Q21$ and $D3Q39$ discrete velocity models and the corresponding weighting functions.

$D2Q21$	$\xi_\alpha = \begin{cases} (0,0), \\ (\pm 1,0),(0,\pm 1) \\ (\pm 1,\pm 1) \\ (\pm 2,0),(0,\pm 2) \\ (\pm 2,\pm 2) \\ (\pm 3,0),(0,\pm 3) \end{cases}$	$\omega_\alpha = \begin{cases} 91/324 \\ 1/12 \\ 2/27 \\ 7/360 \\ 1/432 \\ 1/1620 \end{cases}$	$\alpha = \begin{cases} 0 \\ 1-4 \\ 5-8 \\ 9-12 \\ 13-16 \\ 17-20 \end{cases}$
$D3Q39$	$\xi_\alpha = \begin{cases} (0,0,0), \\ (\pm 1,0,0),(0,\pm 1,0),(0,0,\pm 1) \\ (\pm 1,\pm 1,\pm 1) \\ (\pm 2,0,0),(0,\pm 2,0),(0,0,\pm 2) \\ (\pm 2,\pm 2,\pm 2) \\ (\pm 3,0,0),(0,\pm 3,0),(0,0,\pm 3) \end{cases}$	$\omega_\alpha = \begin{cases} 1/12 \\ 1/12 \\ 1/27 \\ 2/135 \\ 1/432 \\ 1/1620 \end{cases}$	$\alpha = \begin{cases} 0 \\ 1-6 \\ 7-14 \\ 15-20 \\ 21-32 \\ 33-38 \end{cases}$

$$F_\alpha(\mathbf{x},t) = \omega_\alpha \rho \left\{ \left[\frac{\boldsymbol{\xi}_\alpha \cdot \mathbf{a}}{RT} \left(1 + \frac{\boldsymbol{\xi}_\alpha \cdot \mathbf{u}}{RT} \right) - \frac{\mathbf{a} \cdot \mathbf{u}}{RT} \right] + \frac{1}{2\rho RT} [\sigma_{ij} + \rho \mathbf{u}^2] : \left[\frac{(\boldsymbol{\xi}_\alpha \cdot \mathbf{a})}{(RT)} H^{(2)} \left(\frac{\boldsymbol{\xi}_\alpha}{RT} \right) - 2 \frac{\mathbf{a} \boldsymbol{\xi}_\alpha}{RT} \right] \right\}, \tag{9}$$

where $\sigma_{ij} = \Sigma_{\alpha=0}^{d} f'_\alpha \boldsymbol{\xi}_{\alpha i} \boldsymbol{\xi}_{\alpha j}$ is the stress tensor and $f'_\alpha = f_\alpha - f_\alpha^{(0)}$ is the nonequilibrium part of the distribution function f_α. The choice of $\boldsymbol{\xi}_\alpha$ depends on the quadrature in evaluating the moments of Eq. (7). In general, the quadrature must be accurate enough so that not only the conservation constraints are preserved, but also necessary symmetry is retained. According to previous work [40], the Gauss-Hermite quadratures employed for solving the third-order truncated system are based on the $D2Q21$ and $D3Q39$ discrete velocity models for the $2D$ and $3D$ Cartesian lattices, respectively. In these two quadratures, the sound speed $c_s = \sqrt{RT}$ is uniquely equal to $\sqrt{2/3}$. The discrete velocities $\boldsymbol{\xi}_\alpha$ and weights ω_α are listed in Table I.

With the above Cartesian quadratures, Eq. (4) can be simply discretized in physical space and time, and yields the following LBE:

$$f_\alpha(\mathbf{x} + \boldsymbol{\xi}_\alpha \delta t, t + \delta t) = f_\alpha(\mathbf{x},t) - \frac{\delta t}{\tau + 0.5\delta t} (f_\alpha(\mathbf{x},t) - f_\alpha^{(0)}(\mathbf{x},t)) + \frac{\tau \delta t}{\tau + 0.5\delta t} F_\alpha(\mathbf{x},t) \tag{10}$$

with the density, velocity, and pressure calculated as

$$\rho = \sum_{\alpha=0}^{d} f_\alpha, \quad \rho \mathbf{u} = \sum_{\alpha=0}^{d} f_\alpha \boldsymbol{\xi}_\alpha + \frac{\delta t}{2} \mathbf{a}, \quad p = \rho c_s^2. \tag{11}$$

III. BOUNDARY CONDITION, RELAXATION TIME, AND REGULARIZATION

In microscale gas flows, the degree of systems deviating from the equilibrium is measured by the Knudsen number. Therefore, in order to use the LBE (10) to model the microscale gas flow systems, it is better to define the relaxation time τ in terms of Kn [27–32,35,36,38–40,42,43]. On the other hand, when solid wall boundaries are presented, the slip boundary condition should be imposed [27–33,35,39,41–43] and its effects on the relaxation time should be reflected [2,29]. Furthermore, as seen from the above Gauss-Hermite procedure, the nonequilibrium distribution f'_α generally does not lie in the space spanned by the leading N Hermite orthogonal basis, and therefore the Gauss-Hermite procedure introduces an error to the described fluid systems. When Kn is small, such an error is small and ignorable. However, as Kn increases, the error becomes larger and the correct hydrodynamics of the system will be blurred. To avoid this and improve isotropy of the system, a "regularization" procedure [38,43] is introduced.

A. Diffuse scattering boundary condition

From the kinetic theory, the slip boundary condition in solving the BE (1) is described by the gas-surface interaction law [4,5]. Taking into account the wall type via the nonnegative scattering kernel $R(\boldsymbol{\xi}' - \boldsymbol{\xi}, \mathbf{x}, t)$, representing a probability density that particles colliding the wall with velocity between $\boldsymbol{\xi}'$ and $\boldsymbol{\xi}' + d\boldsymbol{\xi}'$ at location $\mathbf{x}$ and time instance t will be reflected with velocity between $\boldsymbol{\xi}$ and $\boldsymbol{\xi} + d\boldsymbol{\xi}$, the boundary condition for the distribution $f(\mathbf{x}, \boldsymbol{\xi}, t)$ can be given as

$$f(\mathbf{x}, \boldsymbol{\xi}, t) = \int_{c'_n < 0} |c'_n| R(\boldsymbol{\xi}' \to \boldsymbol{\xi}, \mathbf{x}, t) f(\mathbf{x}, \boldsymbol{\xi}', t) d\boldsymbol{\xi}', \tag{12}$$

where $c'_n = (\boldsymbol{\xi}' - \mathbf{u}_w) \cdot \mathbf{n}$, with $\mathbf{n}$ being the unit wall vector normal to the boundary surface and the subscription w meaning the wall. If there is no absorption on the wall, the kernel satisfies the normalization and reciprocity conditions, which are expressed respectively as

$$\int_{c'_n > 0} R(\boldsymbol{\xi}' \to \boldsymbol{\xi}, \mathbf{x}, t) d\boldsymbol{\xi}' = 1, \tag{13}$$

and

$$|c'_n| R(\boldsymbol{\xi}' \to \boldsymbol{\xi}, \mathbf{x}, t) f_w^{(0)}(\mathbf{x}, \boldsymbol{\xi}', t) = |c_n| R(-\boldsymbol{\xi} \to -\boldsymbol{\xi}', \mathbf{x}, t) f_w^{(0)}(\mathbf{x}, \boldsymbol{\xi}, t), \tag{14}$$

where $f_w^{(0)}(\mathbf{x}, \boldsymbol{\xi}, t)$ is the wall equilibrium distribution function. Different types of the scattering kernels express different gas-surface interactions and the most well-known Maxwell's kernel has the following form:

$$R(\boldsymbol{\xi}' - \boldsymbol{\xi}, \mathbf{x}, t) = \frac{1}{\rho} \sqrt{\frac{2\pi}{RT}} f_w^{(0)}(\mathbf{x}, \boldsymbol{\xi}, t). \tag{15}$$

By using the Gauss-Hermite quadrature [40], Eqs. (12)–(14) yield the following Maxwell's diffuse-scattering boundary condition in the LBM frame [30,41,42]:

$$f_\alpha(\mathbf{x},t) = \frac{\sum_{\alpha'} |(\boldsymbol{\xi}'_\alpha - \mathbf{u}_w) \cdot \mathbf{n}| f_{\alpha'}(\mathbf{x},t)}{\sum_{\alpha'} |(\boldsymbol{\xi}'_\alpha - \mathbf{u}_w) \cdot \mathbf{n}| f_{\alpha'}^{(0)}(\mathbf{x},t)} f_{\alpha,w}^{(0)}(\mathbf{x},t),$$

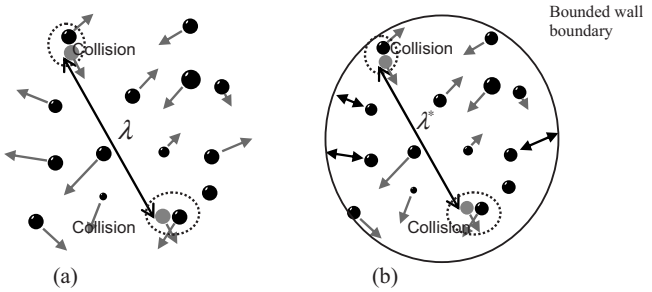

FIG. 1. Definition of molecular mean free path in unbounded and bounded systems. (a) Unbounded system. (b) Bounded system.

$$[(\boldsymbol{\xi}'_\alpha - \mathbf{u}_w)\cdot\mathbf{n} < \mathbf{0};\ (\boldsymbol{\xi}_\alpha \mathbf{u}_w)\cdot\mathbf{n} > \mathbf{0}], \tag{16}$$

where $f^{(0)}_{\alpha,w}(\mathbf{x},t)=f^{(0)}_{\alpha}(\rho_w,\mathbf{u}_w,\mathbf{x},t)$. Previous theoretical analysis [42] based on a $2D$ constant density flow along a straight plate has shown that the above equation generates the following higher-order slip boundary condition

$$\mathbf{u}_s - \mathbf{u}_w = \lambda\left(\frac{\partial \mathbf{u}}{\partial \mathbf{n}}\right)_w + \frac{\lambda^2}{2}\left(\frac{\partial \mathbf{u}}{\partial \mathbf{n}}\right)^2_w + \cdots, \tag{17}$$

provided that the Cartesian lattice spacing is in the order of the molecular mean free path.

B. Relaxation time

In kinetic theory [4,5], the relaxation time τ can be defined in terms of viscosity μ as

$$\tau = \frac{\mu}{p}, \tag{18}$$

and the viscosity is proportional to a qualitatively defined molecular mean free path λ, and for hard sphere gases it is expressed as

$$\lambda = \frac{\mu}{p}\sqrt{\frac{\pi}{2RT}}. \tag{19}$$

Consequently, the relaxation time can be further written as

$$\tau = \sqrt{\frac{2}{\pi}}\lambda c_s = \sqrt{\frac{2}{\pi}}\mathrm{Kn}\ c_s H. \tag{20}$$

Here the definition of the sound speed $c_s=\sqrt{RT}$ is used.

It is important to note that the mean free path given by Eq. (19) is only valid for unbounded systems. In a microscale gas flow system confined by the solid boundaries, some molecules will hit walls and their flight paths may be shorter than the molecular mean free path λ defined in the unbounded systems (see Fig. 1). Therefore, the molecular mean free path in a bounded system should be modified to reflect the boundary wall effects [2,29]. Here we use an effective mean free path λ^* to denote the property of gas flows in the bounded system, and it can be formally expressed as

$$\lambda^* = \lambda\Psi(\mathrm{Kn}). \tag{21}$$

Here Kn is still the conventional Knudsen number without boundary effects. Intuitively, when the boundary walls are far away enough (continuum flows), λ^* should approximate to λ and thus satisfies $\lim_{Kn\to 0}\Psi(\mathrm{Kn})=1$. According to previous investigations [2,29], the function Ψ can be best expressed as

$$\Psi(\mathrm{Kn}) = \frac{2}{\pi}\arctan(a\mathrm{Kn}^{-b}), \tag{22}$$

where the coefficients a and b depend on the boundary types. For microscale flows confined between two infinite parallel walls, it is best to set $a=\sqrt{2}$ and $b=3/4$ based on empirical investigation [29]. Accordingly, Eq. (22) gives the effective viscosity and relaxation time as

$$\mu^* = \mu\Psi(\mathrm{Kn}), \tag{23}$$

and

$$\tau^* = \sqrt{\frac{2}{\pi}}\mathrm{Kn}c_s H\Psi(\mathrm{Kn}), \tag{24}$$

respectively.

C. Regularization

The regularization procedure was introduced by Chen *et al.* [38] to guarantee the nonequilibrium moments of the LBM satisfied in the Hermite space. The regularization is implemented before the collision of the particles. In the regularization procedure, the nonequilibrium distribution f'_α is also projected on the N Hermite-truncated basis by using the Gauss-Hermite procedure, and we have

$$\tilde{f}'_\alpha = \omega_\alpha\sum_{n=0}^{N}\frac{1}{n!}a^{(n)}H^{(n)}\left(\frac{\boldsymbol{\xi}_\alpha}{\sqrt{RT}}\right) \tag{25}$$

with the Hermite coefficients $a^{(n)}=\Sigma^d_{\alpha=0}f'_\alpha H^{(n)}(\boldsymbol{\xi}_\alpha/\sqrt{RT})$. Corresponding to the first three Hermite-truncated expansions where the LBE (10) is obtained, Eq. (25) can be written as the following generic form by using the mass and momentum conservations:

$$\tilde{f}'_\alpha = \omega_\alpha\left[\frac{1}{2c_s^2}H^{(2)}\left(\frac{\boldsymbol{\xi}_\alpha}{c_s}\right)\sum_{\alpha=0}^{d}f'_\alpha\boldsymbol{\xi}_{\alpha i}\boldsymbol{\xi}_{\alpha j} + \frac{B}{6c_s^3}H^{(3)}\left(\frac{\boldsymbol{\xi}_\alpha}{c_s}\right)\sum_{\alpha=0}^{d}f'_\alpha\boldsymbol{\xi}_{\alpha i}\boldsymbol{\xi}_{\alpha j}\boldsymbol{\xi}_{\alpha k}\right], \tag{26}$$

where the additional coefficient B is introduced in the second term and is properly given by $B=1-\Psi(\mathrm{Kn})$. Obviously, when Kn goes to zero, the contribution of the third-order nonequilibrium moment vanishes, and the Navier-Stokes order hydrodynamics is recovered.

Mathematically, the regularization procedure serves as a filter and ensures the nonequilibrium distribution remains inside the defined Hermite space by filtering out the higher-order nonequilibrium moments not supported by the defined Hermite basis. Besides improvement of stability and isotropy of the LBE [38], the other significance of the regularization procedure that needs to be addressed here is the Knudsen layer, a region that the non-Newtonian stress/strain-rate rela-

tionship exists, can be given correctly to some extent. This is because the nonlinear fluid behaviors in the Knudsen layer are mostly influenced by the higher-order nonequilibrium moments, and the regularization procedure ensures the consistent description of the higher-order hydrodynamic moments in the LBM frame. With the above regularization, the discrete distribution function f_α can be written as

$$f_\alpha = f_\alpha^{(0)} + \tilde{f}'_\alpha, \tag{27}$$

and the LBE (10) becomes

$$f_\alpha(\mathbf{x} + \boldsymbol{\xi}_\alpha \delta t, t + \delta t) = f_\alpha^{(0)}(\mathbf{x},t) + \frac{\tau - 0.5\delta t}{\tau + 0.5\delta t}\tilde{f}'_\alpha(\mathbf{x},t) + \frac{\tau \delta t}{\tau + 0.5\delta t}F_\alpha(\mathbf{x},t) \tag{28}$$

when the flow system is unbounded.

IV. NUMERICAL ILLUSTRATIONS

To demonstrate advantages of the kinetic LBM introduced above, the planar Couette and force-driven Poiseuille flows for a range of Knudsen numbers are simulated in this section and accuracy of the present method is verified against DSMC approach [44] and the linearized BE method [45]. For convenience, hereafter we shall refer to the method based on Eq. (10) as the LBE method and the one based on Eq. (28) as the LBE-REG method. Both methods employ Eqs. (8), (9), (16), and (24) with the D2Q21 discrete velocity models.

A. Planar Couette flows

We consider a planar Couette flow confined between two plates parallel to the x axis at $y=\pm H$. The upper plate moves with a constant velocity $U_0=0.1$ and the lower plate remains stationary. Initially, a linear velocity distribution is set in the flow field. The diffuse-scattering boundary conditions of Eq. (16) are used to describe the gas-surface interactions on the plates, while periodic boundary conditions are implemented at the inlet and outlet. To demonstrate grid independence, simulations are carried out on three uniform grid sizes of 17×17, 33×33, and 65×65, respectively. Figure 2 illustrates the normalized velocity ($U=u/U_0$) profiles of Kn $=0.1$, 1, and 10 as a function of distance ($Y=y/H$) between the plates at different grid sizes. As shown in this figure, the velocity profiles demonstrate the Knudsen layers near the plates and a linear property inside the domain. With Kn increasing, the Knudsen layers increase. Slip velocities on the plates are also clearly observed for these three Knudsen numbers and their magnitudes increase as Kn becomes larger. Also see in this figure, the results are consistent with each other as the grid size becomes larger than 33×33. Therefore, in the following, the results based on the grid size of 33×33 are shown only.

It is known that the Knudsen layer comes from the nonlinear fluid behaviors near the boundaries. However, from our earlier experiences [30,31], the LBE (10) cannot capture these phenomena and this can be clearly seen from Fig. 3,

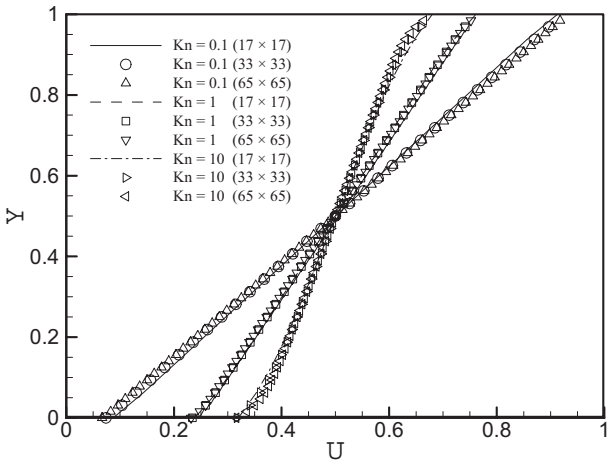

FIG. 2. Normalized velocity profiles for planar Couette flows at different Knudsen numbers and grid sizes.

which compares the normalized velocity profiles of Kn $=0.1$, 1, and 10 between the plates obtained by the LBE and LBE-REG methods. As shown in Fig. 3, the LBE method gives the linear velocity profiles between the plates for all three Knudsen numbers as compared to the LBE-REG solutions. Physically, the nonlinear fluid behaviors of the Knudsen layer are contributions of the high-order nonequilibrium moments. Therefore, we can rationally figure out that the regularization of the nonequilibrium moments makes the LBE well consistent with the coupling physics (Navier-Stokes order hydrodynamics and beyond) at macro and micro scales. The accuracy of the present LBE-REG is shown in Fig. 4, in which the normalized velocity profiles of the planer Couette flows at Kn$=0.1$ and 1 have been compared to the DSMC data [44]. The DSMC method has been generally accepted as an accurate method to model the large Knudsen number flows. Figure 4 shows that the LBE-REG solutions are in good agreement with the DSMC data. The differences between the two simulations imply that more (higher than third-order) terms in the Hermite polynomials should be included in the present LBE-REG model.

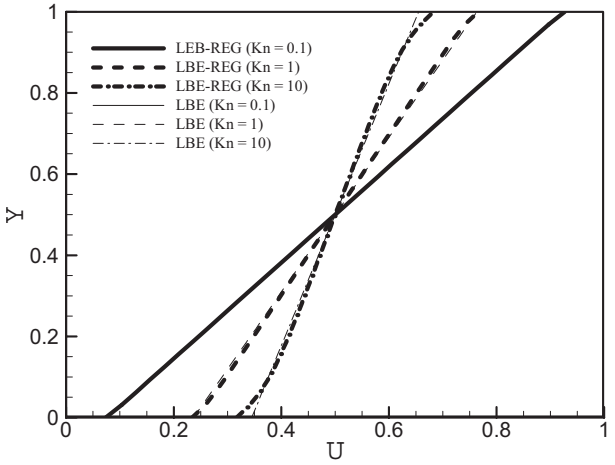

FIG. 3. Regularization effects on the normalized velocity profiles for planar Couette flows at different Knudsen numbers.

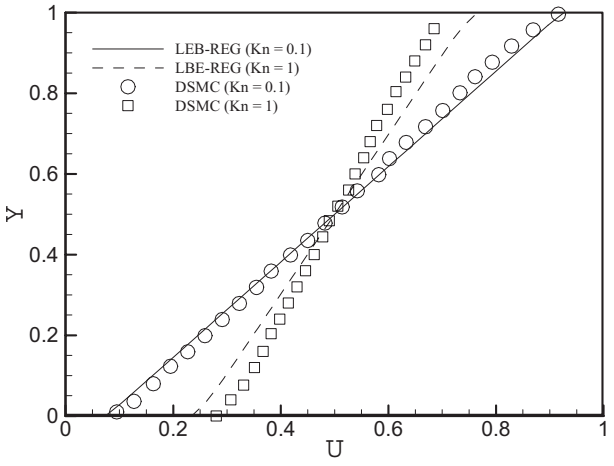

FIG. 4. Comparison of the normalized velocity profiles for planar Couette flows at different Knudsen numbers obtained by the LBE-REG and DSMC approaches.

However, the present method is still shown to be capable of providing a reasonable description for the microscale gas flows.

B. Force-driven Poiseuille flows

The second numerical illustration is the force-driven Poiseuille flows in a $2D$ channel with height H. In numerical simulations, the flow is assumed to be static initially, and a constant force $a=0.01$ is applied in the streamwise direction while periodic boundary conditions are used at the inlet and outlet. To ensure the grid independence of the solutions, two uniform grid sizes of 33×33 and 65×65 are also used for the flows to be presented in the following, and the consistent velocity profile results of the flows at Kn=1 on these two grid sets are displayed in Fig. 5.

Figure 6 shows the normalized velocity profiles, $U=u/U_{\max}$ ($U_{\max}$ is the maximum value in the channel), across the channel for three Knudsen numbers at 0.1, 1, and 10. To show the accuracy of the present method, the DSMC results

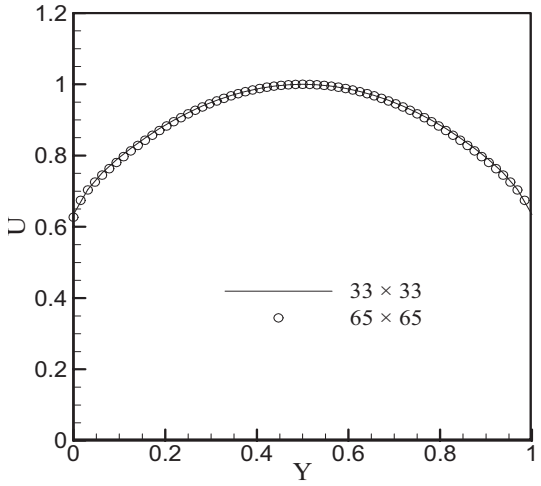

FIG. 5. Normalized velocity profiles for force-driven Poiseuille flows of Kn=1 at different grid sizes.

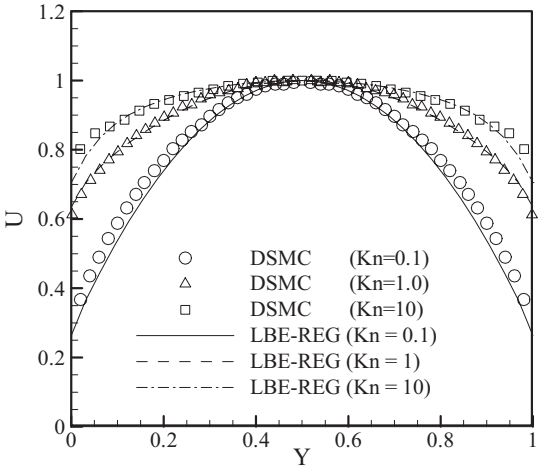

FIG. 6. Comparison of the normalized velocity profiles for force-driven Poiseuille flows at different Knudsen numbers obtained by the LBE-REG and DSMC approaches.

[44] are also included. As observed from this figure, the results obtained by the LBE-REG are in good agreement with the DSMC predictions. With the increase of the Knudsen numbers, the slip velocities at the channel walls increase. As a result, the velocity profiles become flatter and flatter.

One of the major successes in kinetic theory is the prediction of a minimum of the mass flow rate as a function of the Knudsen number at Kn$\sim$1. It was reported in [43] that the LBE model presented in that work can predict the Knudsen minimum. However, the simulations indicate a large difference to the linearized BE and DSMC methods [2,45] due to no consideration of boundary effects on the relaxation time and the third-order nonequilibrium moments. The nondimensionalized mass flow rate, $Q=\Sigma_{y=0}^{H}\rho u(y)/(\rho aH^2/c_s)$, as a function of Knudsen numbers obtained by the present model, is plotted in Fig. 7. For comparison, this figure also includes the DSMC results [2] and the linearized BE solutions [45] as well as the analytical asymptotic expressions in the zero and infinite Knudsen limits [4],

$$Q_0=\sqrt{\pi}/(12\mathrm{Kn})+s_0+(2s_0^2-1)2\mathrm{Kn}/\sqrt{\pi}, \qquad (29a)$$

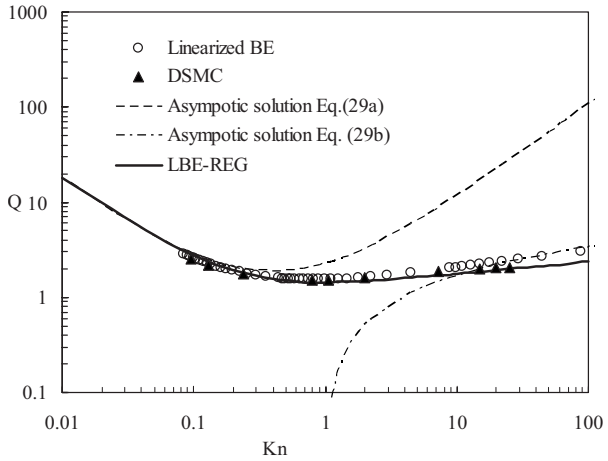

FIG. 7. Nondimensionalized mass flow rate as a function of Knudsen numbers predicted by different methods.

$$Q_\infty = s_\infty \pi^{-1/2} \ln(2\mathrm{Kn}/\sqrt{\pi}), \tag{29b}$$

with $s_0 = 1.01615$ and $s_\infty = 3$. As expected, the LBE-REG predicts a minimum mass flow rate around Kn=1. As Kn decreases to zero limit, all simulation results agree with each other and converge to the asymptotic solutions of Eq. (29a). This implies that Navier-Stokes order hydrodynamics are recovered correctly by all schemes at vanishing Knudsen numbers. At higher Kn, the LBE-REG simulations are close to the asymptotic solution of Eq. (29b) and exhibit an excellent agreement with the results of the linearized BE and DSMC methods, suggesting that the present model with effective relaxation time and modification of the third-order nonequilibrium moments can indeed capture the microscale gas fluid properties at high Knudsen numbers.

V. CONCLUSIONS

In conclusion, a systematic description of the issues of the kinetic lattice Boltzmann method for simulating the microscale gas flows is presented in this paper. By using the Gauss-Hermite quadrature, the diffuse-scattering boundary condition is directly obtained by projecting the Maxwell kinetic boundary condition on the Hermite space. The relaxation time is linked to the Knudsen number, and a concept of the effective mean free path is introduced in determining the relaxation time by taking into account the boundary effects. Significances of the high-order nonequilibrium moments and their regularization procedure are addressed. With a link to the numerical simulations of the Couette and Poiseuille flows, it is argued that by introducing the effective molecular mean free path with boundary effects and regularization procedure to guarantee the nonequilibrium moments of the LBM to be in the Hermite space, the microscale gas flows at a range of the Knudsen numbers can be modeled.

ACKNOWLEDGMENTS

This work were supported by Core Research for Evolutional Science and Technology (CREST) of the Japan Science and Technology (JST) Agency (Grant No: 228205R) and the Japan Society for the Promotion of Science through a Grant-in-Aid for Scientific Research (B) (Grant No. 18360050).

[1] C. M. Huo and Y. C. Tai, Annu. Rev. Fluid Mech. **30**, 579 (1998).
[2] G. K. Karniadakis and A. Beskok, *Microflows: Fundamentals and Simulation* (Springer, New York, 2001).
[3] D. J. Beebe, G. A. Mensing, and G. M. Walker, Annu. Rev. Biomed. Eng. **4**, 261 (2002).
[4] C. Cercignani, *Theory and Application of the Boltzmann Equation* (Scottish Academic Press, Edinburgh, 1975).
[5] S. Chapman and T. G. Cowling, *The Mathematical Theory of Non-Uniform Gases* (Cambridge University Press, Cambridge, England, 1970).
[6] T. Ohwada, Phys. Fluids **8**, 2153 (1996).
[7] G. Bird, *Molecular Gas Dynamics and the Direct Simulation of Gas Flows* (Clarendon Press, Oxford, 1994).
[8] J. H. Ferziger and HG. G. Kaper, *Mathematical Theory of Transport Processes in Gases*, (North-Holland, Amsterdam, 1972).
[9] H. Grad, Commun. Pure Appl. Math. **2**, 331 (1949).
[10] I. Müller and T. Ruggeri, *Rational Extended Thermodynamics* (Springer, New York, 1998).
[11] H. Struchtrup and M. Torrilhon, Phys. Fluids **15**(9), 2668 (2003).
[12] D. A. Wolf-Gladrow, *Lattice-Gas Cellular Automata and Lattice Boltzmann Models* (Springer, Berlin, 2000).
[13] S. Succi, *The Lattice Boltzmann Equation: For Fluid Dynamics and Beyond* (Numerical Mathematics and Scientific Computation Series) (Oxford University Press, New York, 2001).
[14] P. Rosenau, Phys. Rev. A **40**, 7193 (1989).
[15] H. Struchtrup, ZAMP **51**, 346 (2000).
[16] H. Struchtrup, *Some Remarks on the Equations of Burnett and Grad Transport in Transition Regimes*, IMA Volume Series 135 (Springer, New York, 2003).
[17] D. Reitebuch and W. Weiss, Continuum Mech. Thermodyn. **11**, 217 (1999).
[18] U. Frisch, B. Hasslacher, and Y. Pomeau, Phys. Rev. Lett. **56**, 1505 (1986).
[19] S. Wolfram, J. Stat. Phys. **45**, 471 (1986).
[20] G. D. Doolen, *Lattice Gas Methods for Partial Differential Equations* (Addison-Wesley, Reading, PA, 1989).
[21] S. Chen and G. D. Doolen, Annu. Rev. Fluid Mech. **30**, 329 (1998).
[22] X. Shan and H. Chen, Phys. Rev. E **47**, 1815 (1993); X. Shan and H. Chen, Phys. Rev. E **49**, 2941 (1994).
[23] X. Shan and G. Doolen, J. Stat. Phys. **81**, 379 (1995).
[24] S. Chen, H. Chen, D. Martinez, and W. Matthaues, Phys. Rev. Lett. **67**, 3776 (1991).
[25] A. J. C. Ladd, J. Fluid Mech. **271**, 285 (1994); **271**, 311 (1994).
[26] S. Succi, O. Filippova, H. Chen, and S. Orszag, J. Stat. Phys. **107**, 261 (2002).
[27] X. Nie, G. Doolen, and S. Chen, J. Stat. Phys. **107**, 279 (2002).
[28] C. Y. Lim, C. Shu, X. D. Niu, and Y. T. Chew, Phys. Fluids **14**, 2299 (2002).
[29] Z. Guo, T. S. Zhao, and Y. Shi, J. Appl. Phys. **99**, 074903 (2006).
[30] X. D. Niu, C. Shu, and Y. T. Chew, Europhys. Lett. **67**, 600 (2004).
[31] C. Shu, X. D. Niu, and Y. T. Chew, J. Stat. Phys. **121**, 239 (2005).
[32] Y. T. Chew, X. D. Niu, and C. Shu, Int. J. Numer. Methods Fluids **50**, 1321 (2006).
[33] B. Li and D. Kwok, Phys. Rev. Lett. **90**, 124502 (2003).
[34] S. Ansumali and I. V. Karlin, Phys. Rev. Lett. **95**, 260605 (2005).
[35] T. Lee and C. Lin, Phys. Rev. E **71**, 046706 (2005).

[36] Y. H. Zhang, X. J. Gu, R. W. Barber, and D. R. Emerson, Phys. Rev. E **74**, 046704 (2006).
[37] H. Chen, R. Zhang, I. Staroselsky, and M. Jhon, Physica A **362**, 125 (2006).
[38] Y. Zhou, R. Zhang, I. Staroselsky, H. Chen, W. T. Kim, and M. Jhon, Physica A **362**, 68 (2006).
[39] F. Toshi and S. Succi, Europhys. Lett. **69**, 549 (2005).
[40] X. Shan, X. F. Yuam, and H. Chen, J. Fluid Mech. **550**, 413 (2006).
[41] S. Ansumali and I. V. Karlin, Phys. Rev. E **66**, 026311 (2002).
[42] X. D. Niu, C. Shu, and Y. T. Chew, Int. J. Mod. Phys. C **16**, 1927 (2005).
[43] R. Zhang, X. Shan, and H. Chen, Phys. Rev. E **74**, 046703 (2006).
[44] M. J. McNenly, M. A. Gallis, and I. D. Boyd, *Proceedings of the 36th AIAA Thermophysics Conference* (AIAA, Orlando, Florida, 2003).
[45] F. Sharipov and V. Seleznev, J. Phys. Chem. Ref. Data **27**, 657 (1998).